Journal of Materials Chemistry B

PAPER

View Article Online
View Journal | View Issue

Cite this: J. Mater. Chem. B, 2015, 3, 3634

Fabrication of a novel blended membrane with chitosan and silk microfibers for wound healing: characterization, *in vitro* and *in vivo* studies

Zongpu Xu,† Liyang Shi,† Mingying Yang, Haiping Zhang and Liangjun Zhu*‡

Received 31st January 2015,
Accepted 15th March 2015

DOI: 10.1039/c5tb00226e

www.rsc.org/MaterialsB

Pure chitosan membranes present insufficient mechanical properties and a high swelling ratio, which limits their application in biomedical field. In this study, silk microfibers were obtained by chemical hydrolysis, and a novel type of chitosan/silk microfiber (CS/mSF) blended membrane was reported and its multiple physical properties were evaluated. The mechanical properties were significantly improved after blending silk microfibers with a chitosan matrix, while the swelling ratio was decreased. Observation of the surface microstructures of the blended membranes *via* scanning electron microscopy showed abundant embedding of mSF into the CS matrix, as well as connections among mSF. *In vitro* cytocompatibility was also investigated, and the blended membranes exhibited significant cytocompatibility, which was demonstrated by cell proliferation and cell morphology. Furthermore, the *in vivo* healing effects of the blended membrane as a wound dressing were determined on a full-thickness skin wound model of rats. Animal studies revealed that the membranes containing mSF exhibited increased wound healing efficiency compared with pure CS membranes and treatment without wound dressing. From an examination of histological changes, a higher level of epithelialization and collagen formation was observed with treatment of CS/mSF blended membranes after a 21 day repair period. In conclusion, our results indicated that the blended membranes with CS and mSF might be a potential candidate material for wound healing.

1. Introduction

Skin can be easily injured by different causes such as heat, mechanical force, physical and chemical agents, which can be threats to human health. One therapy used for accelerating skin regeneration and reducing scar formation is coverage of the damaged skin with a wound dressing.[1] An ideal wound dressing material should not only act as a barrier against bacteria and dust, but also exhibit good biocompatibility and provide a moist and absorbent environment, as well as control gas permeation, *etc.*[2] Materials derived from biological macromolecules have gained more attention, due to their biocompatibility, biodegradability and renewability.

Chitosan (CS) is a natural macromolecule formed *via* β-(1,4)glycosidic bonds between D-glucosamine and *N*-acetyl-D-glucosamine,[3] which exhibits favorable biocompatibility, biodegradability, antibacterial properties and wound healing effects. CS has currently been studied in tissue engineering, drug delivery, cancer diagnosis, and especially wound healing.[4–8] However, pure CS materials exhibit insufficient mechanical properties and a high swelling ratio. To overcome these limitations, blending CS with other materials to fabricate different forms of wound dressings has become an important methodology.[9–12] Silk fibroin (SF) is a fascinating natural protein extracted from cocoons of the *Bombyx mori* silkworm, which displays excellent mechanical properties, high biocompatibility, controllable biodegradability and remarkable air permeability.[13–15] SF has therefore been adopted as materials for biomedical applications such as tissue engineering and drug delivery,[16–20] as well as wound repair.[21–23] In order to conveniently combine the advantages of CS and SF, previous studies have blended CS with SF solution or lyophilized SF solid to fabricate composite wound dressing materials.[10,24–26] However, the mechanical properties, biological stability and durability of these blended materials indicate that they did not perform very well as wound dressings. Furthermore, the use of crosslinker reagents[3] or toxic organic solvents like HFIP and TFA during the electrospining process[25,26] may present a potential risk.

Silk microfibers (mSF) are prepared directly from degummed silk fibers and have been used as a reinforcement in three-dimensional matrices, like hydrogels and scaffolds, to obtain better mechanical and cellular outcomes.[27–30] Therefore, we hypothesized that a novel

Institute of Applied Bioresource Research, College of Animal Science, Zhejiang University, Hangzhou 310058, PR China. E-mail: ljzhu@zju.edu.cn; Fax: +86 0571 88982185; Tel: +86 0571 88982185

† These authors contributed equally to this work.

‡ Current address: Institute of Applied Bioresource Research, College of Animal Science, Zhejiang University, Room C319, Agriculture Life and Environmental Sciences Building, 866 Yuhangtang Road, Hangzhou 310058, Zhejiang Province, PR China.

wound dressing material could be fabricated by blending CS with mSF, instead of SF solution or lyophilized SF solid. In the current study, different contents of mSF were introduced into a CS matrix to prepare blended membranes and improve the properties of the resulting membranes. Multiple physical properties of the blended membranes, including their mechanical properties, thermal behaviors, swelling ratio and water vapor transmission rate, were rigorously investigated. Furthermore, their *in vitro* cytocompatibility and *in vivo* wound healing effects with and without mSF were comprehensively evaluated on a full-thickness skin wound model in rats. Through this work, we provide valuable insights into the role of mSF in membrane reinforcement and illustrate the increased efficiency of the wound healing effects of CS/mSF blended membranes compared to pure CS membranes *via* both macroscopic and microscopic examination.

2. Results and discussion

2.1 Morphology of mSF and membranes

mSF of different lengths could be obtained by controlling the duration of alkaline hydrolysis. According to SEM images, after hydrolyzing for 6 hours the length of mSF was over 200 μm with significant variations (Fig. 1A), which decreased to 50–200 μm with relative homogeneity after 12 hours (Fig. 1B). Particles with irregular sharp points, instead of microfibers, were developed after 24 hours (Fig. 1C). The alkaline hydrolysis process seemed slower and milder than that reported by Mandal *et al.*,[27] due to the much lower concentration of the NaOH solution. As a reinforcement filler, mSF of different sizes would improve the mechanical properties of a matrix. Here, in order to fabricate uniform blended membranes and to further perform *in vitro* and *in vivo* studies, mSF of 50–200 μm were selected. Photographs of membranes in wet conditions and their surface microstructures are shown in Fig. 2. Pure CS membrane and CS/mSF blended membranes with various mass ratios of mSF exhibited very different morphologies in terms of color, transparency, and surface roughness. CS/mSF blended membranes appeared milk-white in color and exhibited relatively low transmittance compared with the transparent pure CS membrane. Pure CS membrane was so supple as to entirely unfold with tweezers, but the rigidity increased after adding mSF. When the mass ratio was 40%, mSF were dispersed and embedded in the CS matrix, and different degrees of crossing, overlapping and even winding among mSF could also be seen when the ratio reached 60% and 80%, which all resulted in a rough surface in CS/mSF blended membranes.

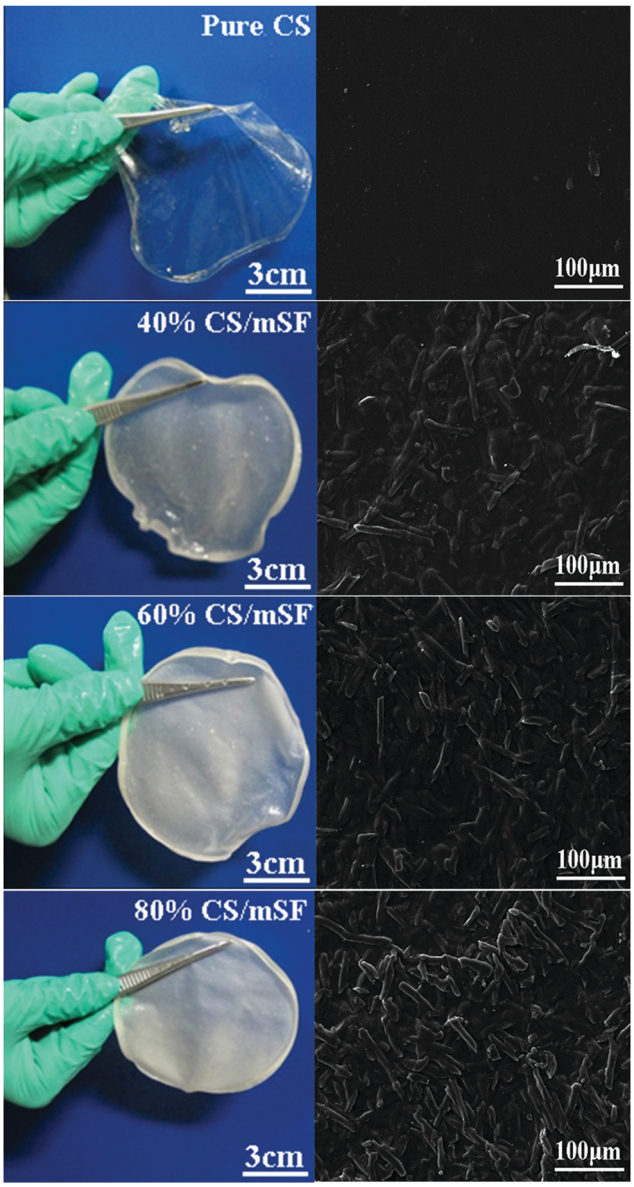

Fig. 2 Digital images (left) and SEM images (right) of membranes (scale bars, 3 cm and 100 μm).

2.2 Mechanical properties of CS/mSF blended membranes

Mechanical properties play important roles in the process of tissue regeneration and further clinical applications.[31] Stress–strain curves of pure CS and CS/mSF blended membranes in

Fig. 1 Silk microfibers with different lengths after alkaline hydrolysis for (A) 6 hours; (B) 12 hours; and (C) 24 hours (scale bar, 100 μm).

wet conditions, together with their elastic modulus, tensile strength, and elongation at break are shown in Fig. 3. Compared with pure CS membrane, the elastic modulus and tensile strength of 40% CS/mSF blended membrane showed little difference. With a further addition of mSF, the elastic modulus and tensile strength of 60% CS/mSF blended membrane significantly increased to 9.96 ± 1.73 MPa and 3.21 ± 0.77 MPa, respectively, and more significantly reached 20.43 ± 2.58 MPa and 3.89 ± 0.71 MPa, respectively, when the mass ratio of mSF reached 80%. The elongation at break also increased to different degrees after adding mSF.

The addition of inorganic fillers, such as carbon nanotubes and hydroxyapatite, has been reported to enhance the mechanical properties of CS matrix materials,[32,33] but these are not biodegradable. Our results demonstrated that natural organic mSF acted effectively as reinforcement fillers to improve the mechanical properties of such biocomposite membranes, so mSF may be a feasible alternative. In this study, mSF were dispersed with random orientations in a CS matrix, indicating anisotropic stress transmission when stretched, which led to no significant improvement in mechanical properties. Apart from the mSF mass ratio, we considered mSF–CS matrix adhesion and interfacial cohesion as contributing factors, but these did not seem obvious in 40% CS/mSF blended membranes. A more interesting feature was the fact that 60% and 80% CS/mSF blended membranes exhibited a many-fold improvement. We thought that with increasing mSF content fiber–fiber interaction, including crossing, overlapping and winding, strengthened, which needed more force to overcome it. According to previous studies,[28,29] biocomposite properties are influenced by fiber content, fiber distribution and fiber-matrix adhesion. Thus one plausible explanation is that the improved mechanical properties were mainly due to interaction among mSF, and partially to mSF–CS matrix adhesion.

2.3 Thermal behaviors of CS/mSF blended membranes

To investigate the thermal behaviors of the membranes and provide information about interaction between CS and mSF, we carried out thermogravimetric analysis (TGA) and differential scanning calorimetry (DSC) analysis. TGA curves of pure CS and CS/mSF blended membranes are presented in Fig. 4A. Two obvious transitions can be observed: the first from 200 °C to 250 °C and the second around 340 °C. By increasing the mSF content, the thermal stability could be gradually enhanced. DSC curves are shown in Fig. 4B, and the exothermic peak at 296 °C would be due to thermal decomposition of amine units of CS.[34] As we know, the thermal decomposition temperature of silk is affected by its structural and morphological properties, like different molecular conformations. The decomposition temperature of well-oriented silk fibers is above 300 °C; the β-sheet structure of silk fibers thermally degrades at 290–295 °C; the α-helix and random coil structures decompose below 290 °C.[35] The blended membranes exhibited an endothermic peak at approximately 322 °C, so we deduced that mSF embedded in the CS matrix were well oriented. No significant difference was observed in the decomposition temperatures of CS/mSF blended membranes with various ratios, indicating physical connections were formed between CS molecules and mSF fillers.

2.4 Swelling ratio and water vapor transmission rate (WVTR) of CS/mSF blended membranes

In the early stages of wound healing, a wound dressing material should be able to absorb exudates released from the wound region and to prevent both excessive dehydration and build-up of exudates. We tested two relevant parameters, swelling ratio and WVTR. As shown in Fig. 5, both the swelling ratio and WVTR of the blended membranes significantly decreased after

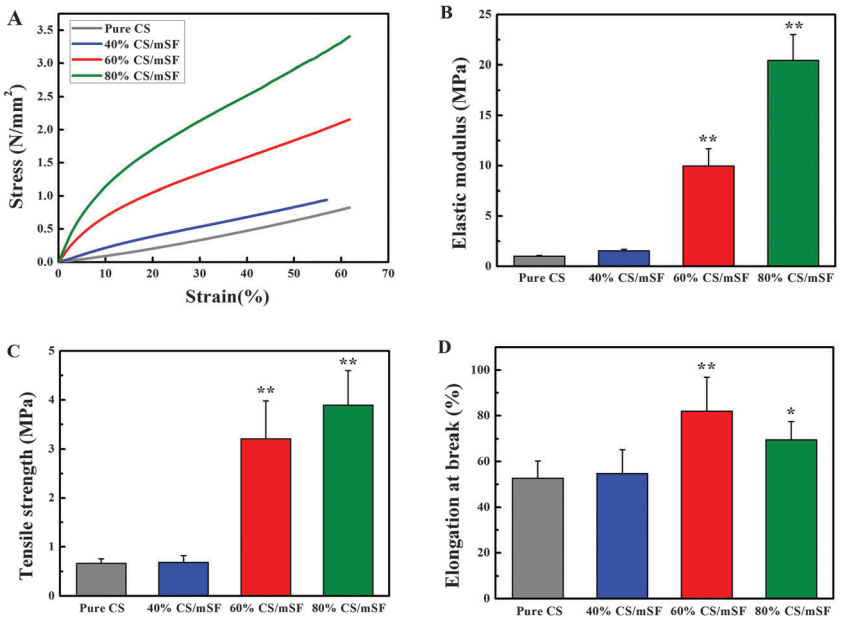

Fig. 3 Mechanical properties of membranes in wet conditions. (A) Stress–strain curves; (B) elastic modulus; (C) tensile strength; (D) elongation at break. Asterisks (*) and (**) mean a statistically significant difference compared to pure CS membrane: *$p < 0.05$ and **$p < 0.01$, $n = 6$.

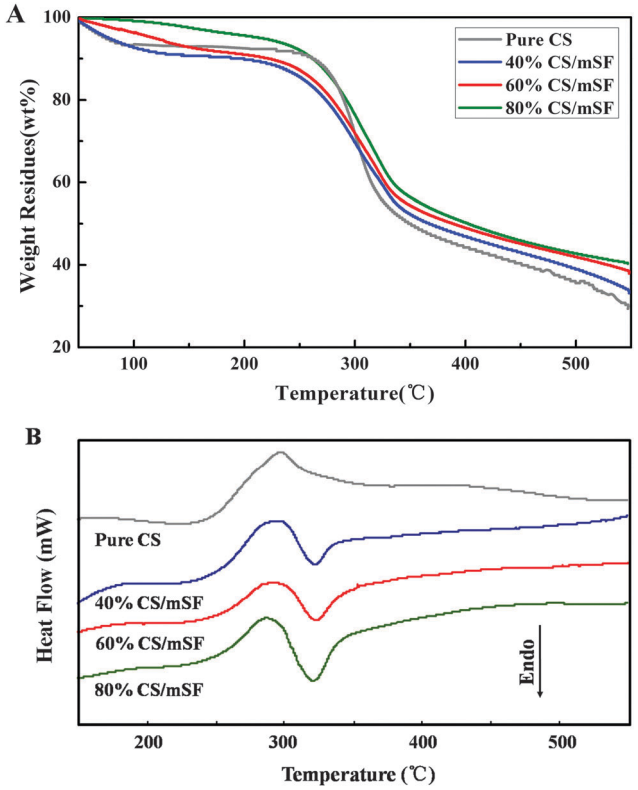

Fig. 4 (A) TGA thermogram curves and (B) DSC curves of membranes.

incorporating mSF, mainly due to the highly hydrophobic crystalline structure of silk fibroin reducing affinity between water molecules and the membranes,[36] thus further decreasing their water uptake and penetration rate. However, blended samples still exhibited a high capability to absorb water, and even the 80% CS/mSF blended membrane reached 2.14 ± 0.72 (g g^{-1}). It is reported that the WVTR of intact skin ranges from 240 to 1920 g m^{-2} per 24 h while that of an uncovered wound is in the order of 4800 g m^{-2} per 24 h.[37] The WVTR of the membranes tested in this study varied from 1209.94 to 1569.66 g m^{-2} per 24 h, similar to that of intact skin and far below that of the blank group, which could not only avoid the risk of wound dehydration but also provide a sufficiently moist environment.

2.5 Cell proliferation and morphology

Non-toxicity and biocompatibility of biomaterials are necessary for future clinical applications. The proliferation and morphology of L929 cells cultured onto pure CS membrane and CS/mSF blended membranes for 1 and 3 days are shown in Fig. 6. L929 cells were able to attach and spread on all types of membranes and the cell number increased gradually with the culture duration, suggesting that the blended membranes exhibited non-cytotoxicity and an ability to support cell proliferation. An MTS assay revealed no significant difference between blended and pure CS membranes, and neither was a definite change seen among blended membranes with different mass ratios of mSF (Fig. 6A). However, according to SEM images (Fig. 6B), the morphology of L929 cells attached to tested membranes exhibited obvious differences at 3 days. For CS/mSF blended membranes, the attached cells displayed a more typically elongated shape and plentiful filopodia could be clearly observed, especially when the mass ratio of mSF was 80%.

The substrate stiffness and surface topography of a material can affect multiple aspects of cells, such as proliferation, migration and differentiation.[38–40] In this study, the embedded mSF in the CS matrix, together with connections among mSF such as crossing and winding, offered attachment and support for L929 cells. The filopodia provided another proof of better morphology, indicating that L929 cells could migrate with the assistance of mSF. These results demonstrated that CS/mSF blended membranes exhibited good cytocompatibility, and the 80% CS/mSF blended membrane could provide the best micro-environment for cell behaviors.

2.6 Wound healing effect

Based on the impressive performance of the blended membranes, we further investigated the wound healing effects of the 80% CS/mSF blended membrane as a wound dressing on rats. Full-thickness skin wound models have generally been utilized to evaluate the wound healing effects of different types of wound dressings.[21,41,42] In this study, circular full-thickness wounds 2 cm in diameter were formed on the backs of rats and covered with pure CS membrane, 80% CS/mSF blended membrane, and vaseline cream as a blank control. Representative photographs of wound healing at time points 0, 7, 14, and 21 days after

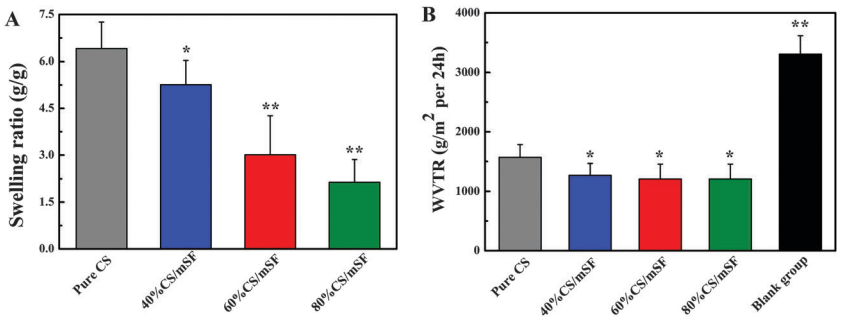

Fig. 5 (A) Swelling ratio and (B) water vapor transmission rate of membranes. Asterisks (*) and (**) mean a statistically significant difference compared to pure CS membrane: * $p < 0.05$ and ** $p < 0.01$, $n = 6$.

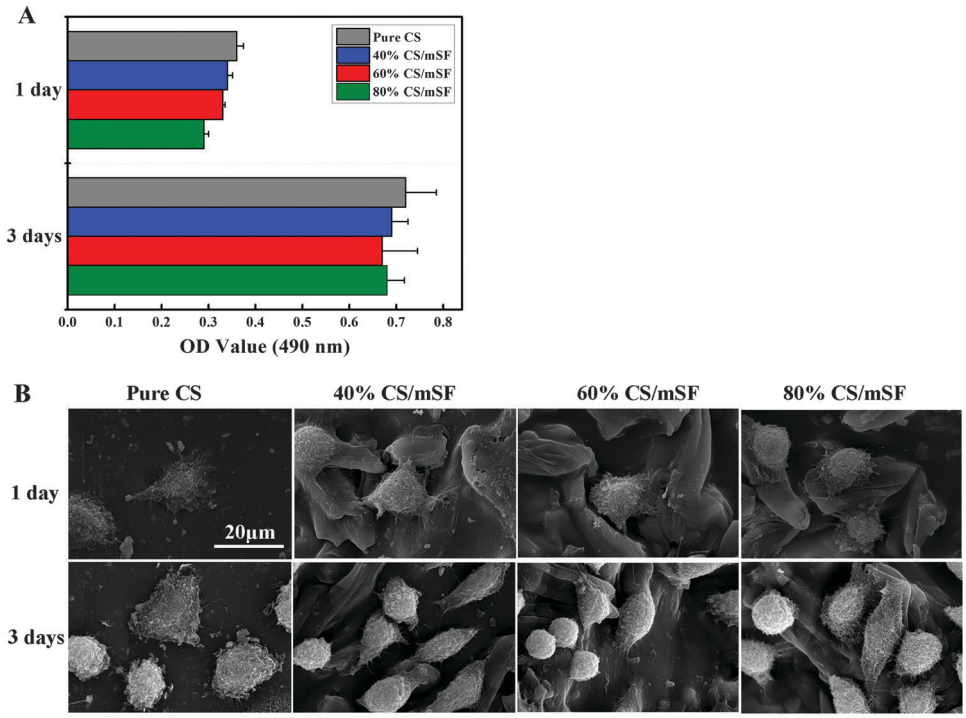

Fig. 6 (A) Proliferation of L929 cells on tested membranes for 1 and 3 days. (B) SEM images of L929 cells cultured onto membranes for 1 and 3 days (scale bar, 20 μm).

different treatments are shown in Fig. 7, and histological changes of wound sections stained with H&E are shown in Fig. 8. During the repair period, the control group without wound dressing displayed the biggest wound size, while the wound area under treatment with wound dressings significantly decreased, indicating improved efficiency. After 7 days, wound areas in the control group increased to 124.68 ± 7.79%, while wound areas covered with pure CS membrane and CS/mSF blended membrane decreased to 54.66 ± 9.22% and 40.73 ± 8.6%, respectively (Fig. 7B). After 14 days, the wound area covered with CS/mSF blended membrane was similar to that with pure CS membrane, but at 21 days the wound area covered with CS/mSF blended membrane was much smaller than that with pure CS membrane and was almost totally closed.

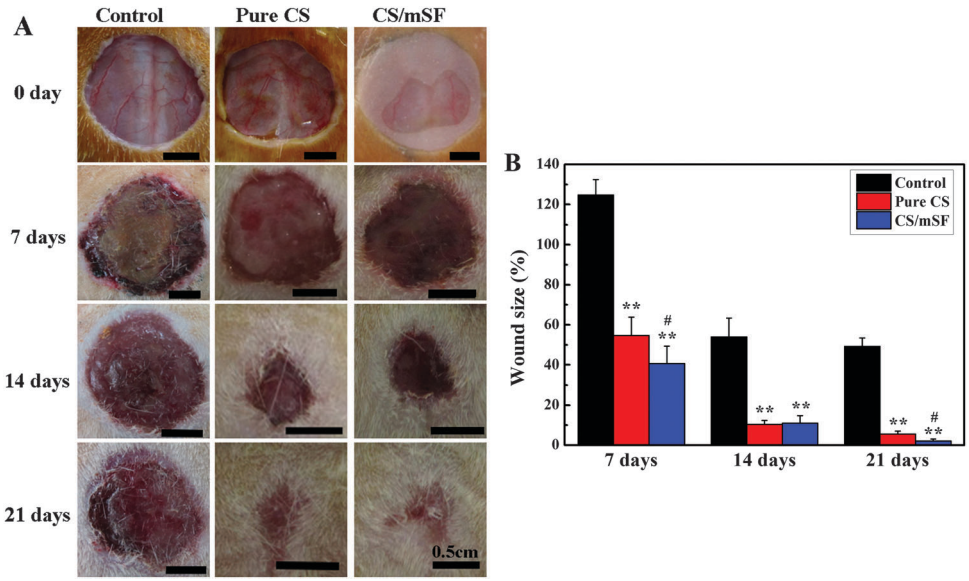

Fig. 7 (A) Digital images of macroscopic wound condition, (scale bar, 0.5 cm). (B) Percentage wound size compared with initial value at day 0. Asterisks (**) mean statistically significant difference compared to control and (#) means statistically significant difference compared to CS, ** $p < 0.01$, # $p < 0.05$, $n = 5$. Control (covered with vaseline cream); pure CS (pure CS membrane); CS/mSF (80% CS/mSF blended membrane).

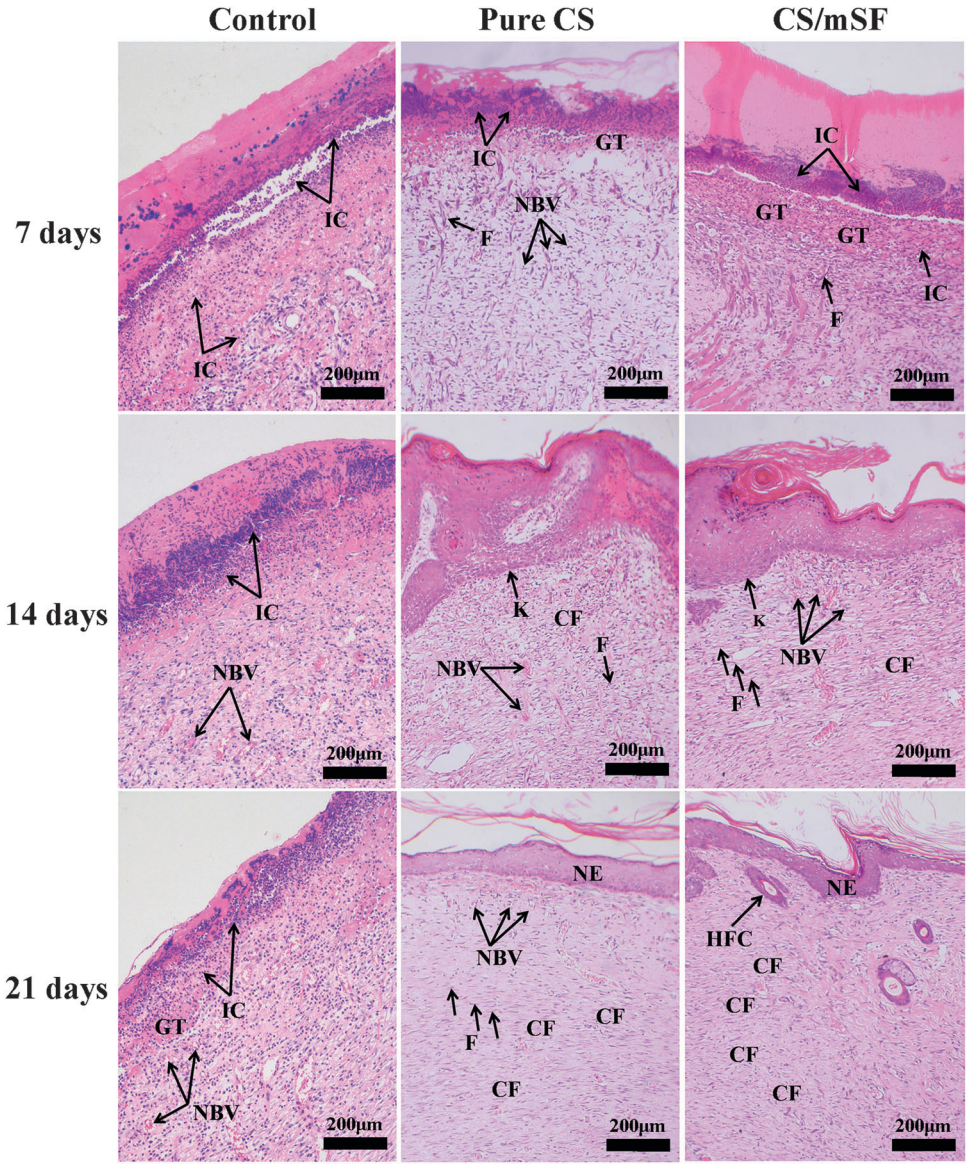

Fig. 8 Histological images of wound sections stained with H&E. IC: inflammatory cells; GT: granulation tissue; F: fibroblasts; K: keratinocytes; NBV: new blood vessels; CF: collagen fiber; NE: new epithelium; HFC: hair follicle cells. Control (covered with vaseline cream); pure CS (pure CS membrane); CS/mSF (80%CS/mSF blended membrane).

Skin wound healing is a complicated process involving various cells and growth factors, which roughly involves four phases: hemostasis, inflammation, proliferation and remodeling.[43] Inflammation could be generated once the injury was created, and intensified after foreign materials adhered to the wound. At 7 days, injured skin covered with pure CS membrane displayed a red color with a smooth outline on the contact interface, while the wound area treated with CS/mSF blended membrane was red-brown and the outline was clearly rough (Fig. 7A). Silk fibroin has been recognized as non-toxic and less inflammatory,[44,45] but tissue edema was seen around parts of the wound in the CS/mSF blended membrane group (Fig. 7A). This may be a consequence of the medium being mixed, as pure CS membrane was a smooth single-phase system while CS/mSF blended membrane was a rough two-phase system. As a result, the inflammation process would be more intense and time-consuming, which could be reflected by inflammatory cells appearing in large quantities, mainly distributed at the border of the wound and the biomaterials at 7 days (Fig. 8). From histological observation, granulation tissue also appeared in the wound dressing treatment groups, but the amount was much greater in the CS/mSF blended membrane group. At 14 days, the wound color tended to become lighter and inflammatory cells were significantly decreased. Many new blood vessels could be seen in all groups, which were essential for continuation of the process. At 21 days, the newly generated skin had a similar color to normal skin and blood vessels decreased, while it seemed there was no obvious change in the control group. One notable difference was that hair follicle cells could be observed in the CS/mSF blended membrane

group (Fig. 7A). Fibroblasts uniformly distributed in better order, and considerable collagen deposition indicated partial recovery of normal structure and function.

Chitosan could activate macrophages, thus helping fibroblast proliferation and collagen synthesis,[46] and this promoted the appearance and maturation of granulation tissue. Silk fibroin has been confirmed to boost epithelialization in several studies.[2,31,47,48] We deduced that with continuous epithelialization CS and mSF exerted a synergistic effect. To summarize, we firmly believe that CS/mSF blended membrane achieved the best wound healing efficiency, as at the macroscopic level the wound size was the smallest and at the microscopic level tissue was completely repaired. Therefore, silk microfibers embedded in a CS matrix improved wound healing at both macroscopic and microscopic levels. There is also a need to evaluate other relevant indices to explain and clarify the details of wound healing.

3. Conclusion

Various lengths of mSF could be obtained by control of the duration of alkaline hydrolysis. With the addition of mSF as a reinforcement to a CS matrix, high-performance blended membranes were fabricated, especially with significantly improved mechanical properties. CS/mSF blended membranes also exhibited a suitable swelling ratio and WVRT, which are essential for an ideal wound dressing material. The result of *in vitro* cell experiments indicated that CS/mSF blended membranes displayed good cytocompatibility. Silk microfibers embedded in a CS matrix showed improved repair efficiency for full-thickness wounds *in vivo* in both macroscopic and microscopic aspects. In conclusion, our results demonstrate a blended membrane with CS and SF microfibers would be a promising candidate for use as a wound dressing.

4. Experimental section

4.1 Materials

Silk cocoons of the silkworm *Bombyx mori* were provided by the Institute of Huzhou Cocoon Testing (PR China). Chitosan (degree of deacetylation: 90–95%) was purchased from Shanghai Sangon Biotech Co., Ltd. Mouse fibroblast-like cells (L929) were purchased from the Shanghai Institutes for Biological Sciences, Chinese Academy of Sciences. Fetal bovine serum (FBS), trypsinase, high-glucose Dulbecco's modified Eagle's medium (DMEM), penicillin, and streptomycin were purchased from GIBCO. Phosphate buffered saline (PBS) solution was purchased from Jinuo Biopharma Technology Co., Ltd. Sprague-Dawley rats were purchased from Zhejiang Province Laboratory Animal Center. Hematoxylin was purchased from SIGMA, and eosin was from Shanghai Maikun Chemical Co., Ltd. All reagents were of analytical grade and were used as received without any further purification.

4.2 Preparation of silk microfibers (mSF)

mSF were prepared as described by a previous report, with some modifications.[27] In brief, 10 g cut pieces of silk cocoons were boiled for 30 minutes in 1000 mL 0.5 wt% Na_2CO_3 solution to degum them and rinsed thoroughly with deionized water, repeating this degumming process once, and then air-dried. To obtain silk microfibers of different lengths, we immersed degummed silk in 1 mol L^{-1} NaOH solution for 6, 12 and 24 hours at room temperature. The alkaline hydrolysis was stopped by excess deionized water and the silk microfibers were washed 5 times to remove residual NaOH. Dried mSF from wet silk slurry were prepared using a hot-air dryer.

4.3 Preparation of CS/mSF blended membranes

2% (w/v) CS solution was first prepared by dissolving CS in 0.3 mol L^{-1} acetic acid. Then mSF were added to the CS solution and mixed using magnetic stirring for 10 minutes to obtain a homogeneous composite solution. The mass ratios of mSF to CS were stipulated as 0, 40, 60, and 80 wt%. Pure CS membrane and CS/mSF blended membranes were developed by evaporation overnight at room temperature from the above solution. Then the membranes were immersed in 0.1 mol L^{-1} NaOH methanol solution for 6 hours to insolubilize them, and finally the membranes were washed with deionized water to remove methanol residues.

4.4 Characterization of pure CS membrane and CS/mSF blended membranes

4.4.1 Scanning electron microscopy (SEM). A scanning electron microscope (XL30-ESEM, Philips, The Netherlands) with an accelerating voltage of 20 kV was used to observe the morphology of mSF and membrane samples. Before observing, all samples were in a totally dry state and sputtered with gold ions.

4.4.2 Mechanical properties. Membrane samples were cut into 50 × 8 mm strips and soaked in deionized water for 2 hours to balance them prior to testing. A universal tester (AGS-J, Shimadzu, Japan) equipped with a 50 N capacity load cell was utilized to measure mechanical properties of the wet membranes. All the tests were controlled by a model at a speed of 3 mm min^{-1}. The data for elastic modulus, tensile strength and elongation at break were reported from the stress–strain curves as means ± SD (n = 6).

4.4.3 Thermogravimetric analysis (TGA). A TGA instrument (DTG-60A, Shimadzu, Japan) was used for thermogravimetric analysis of membranes. The tests were performed under a nitrogen atmosphere (50 mL min^{-1}) and the temperature was increased from 50 to 550 °C with a ramp rate of 10 °C min^{-1}. The results were obtained by the software OriginPro 8.5.

4.4.4 Differential scanning calorimetry (DSC). The thermal behaviors of membrane samples were determined using a DSC analyzer (822e, Mettler Toledo, Switzerland) under a nitrogen gas flow rate of 80 mL min^{-1}. The test temperature ranged from 150 to 550 °C at a heating rate of 10 °C min^{-1}.

4.4.5 Swelling ratio. The swelling ratio was tested following the reported method.[49] Membrane samples were cut into 30 × 30 mm pieces and immersed in deionized water overnight. The wet weight of a piece (W_s) was obtained after removing the excess water on the surface. The samples were dried in an oven

at 50 °C for 6 hours and the dried weight of a piece was measured (W_d). The swelling ratio (g g^{-1}) was calculated by the following formula:

$$\text{Swelling ratio} = (W_s - W_d)/W_d$$

The result was given as means ± SD (n = 6).

4.4.6 Water vapor transmission rate (WVTR) assay. The WVTR assay followed our previous report.[50] In brief, the tested membranes were fixed on the opening of a bottle (14 mm diameter) containing 10 mL deionized water. The initial weight of the bottle was W_1 (g). Then the bottle was placed into an incubator with 39 ± 2% relative humidity at 38 ± 0.5 °C for 4 days. Afterwards the bottle was weighed at W_2 (g). The open bottle acted as the blank group. The WVTR of the membrane was then calculated by the following formula:

$$Q = (W_1 - W_2)/4S$$

where Q represents the WVTR (g m^{-2} per 24 h) and S is the area of the bottle opening (m^2). The result was given as means ± SD (n = 6).

4.5 *In vitro* cell experiment

Cell proliferation on the membranes was detected using mouse fibroblast-like cells (L929) by a 3-(4,5-dimethylthiazol-2-yl)-5-(3-carboxymethoxyphenyl)-2-(4-sulfophenyl)-2*H*-tetrazolium (MTS) assay. Pure CS membranes and blended CS/mSF membranes were cut into circular pieces with diameters of 6.4 mm, which were then sterilized by 70% ethanol and UV irradiation. Sterilized membrane samples were placed into 96-well plates, then 200 μL cell suspension containing 5×10^3 cells was seeded onto each membrane. Complexes of cells and membranes were incubated at 37 °C in a humidified atmosphere with 5% CO_2 for 1 and 3 days. The cell culture medium with 10% FBS, 100 U mL^{-1} penicillin and 100 μg mL^{-1} streptomycin was refreshed every 2 days. At the appointed time, cell proliferation was evaluated using an MTS kit (Promega, USA) according to the manufacturer's protocol. In brief, 100 μL cell culture medium was removed, 20 μL MTS reagent was added to each well and the plates were incubated at 37 °C for 4 hours. The optical density (OD) of each sample was determined at 490 nm using a microplate reader (PLUS 384, Molecular Devices, USA).

SEM was utilized to observe the morphology of cells on membranes. Before SEM measurement, seeded membranes were fixed with 2.5% glutaraldehyde and 2.5% osmic acid in PBS solution for 3 hours each at 4 °C. The fixed membranes were dehydrated in increasing concentrations of ethanol (30, 50, 70, 85, 95 and 100%) for 20 minutes each, and then critical-point dried. The dried samples were coated with gold ions by sputtering and observed using SEM (S-3000N, Hitachi, Japan).

4.6 *In vivo* wound healing study

4.6.1 Full-thickness skin wound model of rats. Healthy Sprague-Dawley rats (male, weighing 200 to 220 g) were used to form full-thickness skin wound models. In detail, the surgical areas were shaved with an electric razor one day before the operation. After anesthesia with an intraperitoneal injection of 10% chloral hydrate (3.5 mL kg^{-1} body weight), the operation site, back skin centered on the spine, was cleaned with 70% ethanol and iodine. Then a circular full-thickness wound 2 cm in diameter was made, referring to a template line, and the tissue excised to the panniculus carnosus layer. The 45 treated rats were divided randomly into three groups, corresponding to a control group, a pure CS membrane group and an 80% CS/mSF blended membrane group, respectively. The wounds of the control group were smeared with vaseline cream, while those of the experiment groups were covered with CS pure membrane and 80% CS/mSF blended membrane. In addition, above the membranes sterilized gauze was sewn around the skin to prevent the dressings from falling off. We confirm that all animal experiments in our study were carried out in accordance with the guidelines and approval (ZJU2015-474-02) of the Laboratory Animal Welfare Ethics Committee of Zhejiang University.

4.6.2 Measurement of wound percentage size. The wound region was photographed with a measuring scale at 7, 14 and 21 days using a digital camera (Canon IXUS 610, Japan) and in each group 5 rats were measured at one time point. The wound area was measured by MapInfo Professional 10.0 software, and then the wound size was calculated compared to the initial state. The result was given as means ± SD (n = 5).

4.6.3 Histological evaluation. The regenerated tissue at the wounds, together with the surrounding uninjured skin, was excised at 7, 14 and 21 days, as well as normal skin, fixed in 10% phosphate-buffered formalin, and then embedded in a paraffin block. Sections of 4 μm thickness were prepared by a rotary microtome (RM2135, Leica, Germany) and stained with hematoxylin and eosin (H&E) reagents according to routine procedures. Histological changes were observed using a microscope (BH2, Olympus, Japan).

4.7 Statistical analysis

All data were given as means ± SD (n = 5–6). Statistical analyses were carried out using SPSS 16.0 software. Statistically significant differences (* $p < 0.05$, ** $p < 0.01$ or # $p < 0.05$) were determined by one-way ANOVA with Student's t-test.

Acknowledgements

This study is supported by the earmarked fund (CARS-22-ZJ0402) for China Agriculture Research System (CARS) and National Natural Science Foundation of China (21172194). We would like to thank Yu Zhu for revision of the manuscript.

References

1 R. Fu, C. Li, C. Yu, H. Xie, S. Shi, Z. Li, Q. Wang and L. Lu, *Drug Delivery*, 2014, 1–12.
2 A. Vasconcelos, A. C. Gomes and A. Cavaco-Paulo, *Acta Biomater.*, 2012, **8**, 3049–3060.
3 Z. Gu, H. Xie, C. Huang, L. Li and X. Yu, *Int. J. Biol. Macromol.*, 2013, **58**, 121–126.

4 R. Jayakumar, D. Menon, K. Manzoor, S. Nair and H. Tamura, *Carbohydr. Polym.*, 2010, **82**, 227–232.
5 I. Y. Kim, S. J. Seo, H. S. Moon, M. K. Yoo, I. Y. Park, B. C. Kim and C. S. Cho, *Biotechnol. Adv.*, 2008, **26**, 1–21.
6 S. K. L. Levengood and M. Zhang, *J. Mater. Chem. B*, 2014, **2**, 3161–3184.
7 D. Archana, J. Dutta and P. Dutta, *Int. J. Biol. Macromol.*, 2013, **57**, 193–203.
8 D. Archana, B. K. Singh, J. Dutta and P. Dutta, *Carbohydr. Polym.*, 2013, **95**, 530–539.
9 M. Y. Bai, T. C. Chou, J. C. Tsai and W. C. Yu, *J. Biomed. Mater. Res., Part A*, 2014, **102**, 2324–2333.
10 E. Lih, J. S. Lee, K. M. Park and K. D. Park, *Acta Biomater.*, 2012, **8**, 3261–3269.
11 A. Hashemi Doulabi, H. Mirzadeh, M. Imani and N. Samadi, *Carbohydr. Polym.*, 2013, **92**, 48–56.
12 H. F. Shi, X. G. Wang, S. C. Wu, Z. W. Mao, C. G. You and C. M. Han, *J. Mech. Behav. Biomed. Mater.*, 2014, **29**, 114–125.
13 Y. Cao and B. Wang, *Int. J. Mol. Sci.*, 2009, **10**, 1514–1524.
14 Z. Shao and F. Vollrath, *Nature*, 2002, **418**, 741.
15 B. D. Lawrence, J. K. Marchant, M. A. Pindrus, F. G. Omenetto and D. L. Kaplan, *Biomaterials*, 2009, **30**, 1299–1308.
16 B. Kundu, R. Rajkhowa, S. C. Kundu and X. Wang, *Adv. Drug Delivery Rev.*, 2013, **65**, 457–470.
17 E. M. Pritchard and D. L. Kaplan, *Expert Opin. Drug Delivery*, 2011, **8**, 797–811.
18 H. Lee, C. H. Jang and G. H. Kim, *J. Mater. Chem. B*, 2014, **2**, 2703–2713.
19 A. R. Murphy and D. L. Kaplan, *J. Mater. Chem.*, 2009, **19**, 6443–6450.
20 A. S. Mehta, B. K. Singh, D. Archana, K. Snigdha, R. Harniman, S. S. Rahatekar, R. Tewair and P. Dutta, *J. Biomater. Appl.*, 2015, **29**, 1314–1325.
21 D. H. Roh, S. Y. Kang, J. Y. Kim, Y. B. Kwon, H. Young Kweon, K. G. Lee, Y. H. Park, R. M. Baek, C. Y. Heo, J. Choe and J. H. Lee, *J. Mater. Sci.: Mater. Med.*, 2006, **17**, 547–552.
22 R. Okabayashi, M. Nakamura, T. Okabayashi, Y. Tanaka, A. Nagai and K. Yamashita, *J. Biomed. Mater. Res., Part B*, 2009, **90**, 641–646.
23 Z. Karahaliloglu, B. Ercan, E. B. Denkbas and T. J. Webster, *J. Biomed. Mater. Res., Part A*, 2015, **103**, 135–144.
24 W. Luangbudnark, J. Viyoch, W. Laupattarakasem, P. Surakunprapha and P. Laupattarakasem, *Sci. World J.*, 2012, **2012**, 697201.
25 Z. X. Cai, X. M. Mo, K. H. Zhang, L. P. Fan, A. L. Yin, C. L. He and H. S. Wang, *Int. J. Mol. Sci.*, 2010, **11**, 3529–3539.
26 K. H. Zhang, Q. Z. Yu and X. M. Mo, *Int. J. Mol. Sci.*, 2011, **12**, 2187–2199.
27 B. B. Mandal, A. Grinberg, E. S. Gil, B. Panilaitis and D. L. Kaplan, *Proc. Natl. Acad. Sci. U. S. A.*, 2012, **109**, 7699–7704.
28 S. Yodmuang, S. L. McNamara, A. B. Nover, B. B. Mandal, M. Agarwal, T. A. Kelly, P. H. Chao, C. Hung, D. L. Kaplan and G. Vunjak-Novakovic, *Acta Biomater.*, 2015, **11**, 27–36.
29 S. Mobini, B. Hoyer, M. Solati-Hashjin, A. Lode, N. Nosoudi, A. Samadikuchaksaraei and M. Gelinsky, *J. Biomed. Mater. Res., Part A*, 2013, **101**, 2392–2404.
30 S. D. McCullen, C. M. Haslauer and E. G. Loboa, *J. Mater. Chem.*, 2010, **20**, 8776–8788.
31 B. K. Gu, S. J. Park, M. S. Kim, C. M. Kang, J. I. Kim and C. H. Kim, *Carbohydr. Polym.*, 2013, **97**, 65–73.
32 S. F. Wang, L. Shen, W. D. Zhang and Y. J. Tong, *Biomacromolecules*, 2005, **6**, 3067–3072.
33 Q. Hu, B. Li, M. Wang and J. Shen, *Biomaterials*, 2004, **25**, 779–785.
34 L. S. Guinesi and É. T. G. Cavalheiro, *Thermochim. Acta*, 2006, **444**, 128–133.
35 M. A. de Moraes and M. M. Beppu, *J. Appl. Polym. Sci.*, 2013, **130**, 3451–3457.
36 C. Z. Zhou, F. Confalonieri, M. Jacquet, R. Perasso, Z. G Li and J. Janin, *Proteins*, 2001, **44**, 119–122.
37 N. L. Yusof, A. Wee, L. Y. Lim and E. Khor, *J. Biomed. Mater. Res., Part A*, 2003, **66**, 224–232.
38 B. D. Lawrence, Z. Pan and M. I. Rosenblatt, *PLoS One*, 2012, **7**, e50190.
39 X. Hu, S. H. Park, E. S. Gil, X. X. Xia, A. S. Weiss and D. L. Kaplan, *Biomaterials*, 2011, **32**, 8979–8989.
40 D. E. Discher, P. Janmey and Y. L. Wang, *Science*, 2005, **310**, 1139–1143.
41 S. Kanokpanont, S. Damrongsakkul, J. Ratanavaraporn and P. Aramwit, *Int. J. Pharm.*, 2012, **436**, 141–153.
42 E. S. Gil, B. Panilaitis, E. Bellas and D. L. Kaplan, *Adv. Healthcare Mater.*, 2013, **2**, 206–217.
43 R. F. Diegelmann and M. C. Evans, *Front. Biosci.*, 2004, **9**, 283–289.
44 G. H. Altman, F. Diaz, C. Jakuba, T. Calabro, R. L. Horan, J. Chen, H. Lu, J. Richmond and D. L. Kaplan, *Biomaterials*, 2003, **24**, 401–416.
45 L. Meinel, S. Hofmann, V. Karageorgiou, C. Kirker-Head, J. McCool, G. Gronowicz, L. Zichner, R. Langer, G. Vunjak-Novakovic and D. L. Kaplan, *Biomaterials*, 2005, **26**, 147–155.
46 R. Jayakumar, M. Prabaharan, P. T. Sudheesh Kumar, S. V. Nair and H. Tamura, *Biotechnol. Adv.*, 2011, **29**, 322–337.
47 A. Sugihara, K. Sugiura, H. Morita, T. Ninagawa, K. Tubouchi, R. Tobe, M. Izumiya, T. Horio, N. G. Abraham and S. Ikehara, *Proc. Soc. Exp. Biol. Med.*, 2000, **225**, 58–64.
48 K. Zhang, Y. Qian, H. Wang, L. Fan, C. Huang, A. Yin and X. Mo, *J. Biomed. Mater. Res., Part A*, 2010, **95**, 870–881.
49 S. Yan, Q. Zhang, J. Wang, Y. Liu, S. Lu, M. Li and D. L. Kaplan, *Acta Biomater.*, 2013, **9**, 6771–6782.
50 S. Min, X. Gao, C. Han, Y. Chen, M. Yang, L. Zhu, H. Zhang, L. Liu and J. Yao, *J. Biomater. Sci., Polym. Ed.*, 2012, **23**, 97–110.

